Measurements of the spin-correlation parameters A_{00kk}, A_{00ks}, and A_{00ss} in p-p elastic scattering between 400 and 600 MeV

E. Aprile,* R. Hausammann,† E. Heer, R. Hess, C. Lechanoine-Leluc,
W. R. Leo, S. Morenzoni, Y. Onel, and D. Rapin
Departement de Physique Nucléaire et Corpusculaire, University of Geneva, 1211 Geneva 4, Switzerland

S. Mango
Schweizerisches Institut fur Nuklearforschung, 5234 Villigen, Switzerland
(Received 22 Februrary 1983)

We have measured the spin-correlation parameters A_{00kk}, A_{00ks}, and A_{00ss} in p-p scattering between 400 and 600 MeV using a longitudinally polarized beam and a butanol target polarized in the horizontal plane. Owing to the restrictive geometrical acceptance of the target, the polarization axis of the target was oriented at an angle α with respect to beam direction. The parameters A_{00kk} and A_{00ks} were therefore measured as a linear combination at 577, 536, 514, 494, and 445 MeV. These experiments were extended to the measurement of A_{00ks} and A_{00ss} by using a transversely polarized beam. We present the results, which are compared with phase-shift predictions.

I. INTRODUCTION

Proton-proton scattering experiments constitute one of the most direct ways of studying the force between two nucleons. At intermediate energies, the spin-dependent scattering amplitudes are large and of the same magnitude as the spin-independent amplitudes. The spin-averaged total cross section rises with energy, π-production thresholds open at 290 MeV, and spin-dependent effects vary rapidly with scattering angle and energy.

The measurement of the p-p total-cross-section difference with longitudinally polarized beam and target by the Argonne group[1-3] suggests the existence of two-nucleon resonances. The structure observed in these measurements was recently confirmed by the measurements of the Geneva-Saclay-SIN collaboration.[4] However, if these resonances really exist, they are most probably connected to the N-Δ system because of their large widths.

As in other areas of hadronic physics, the most exciting recent results have been in the region of large transverse momentum. In particular, the large value of A_{00nn} observed at Argonne[5] in p-p elastic scattering near $\theta_{\text{c.m.}}=90°$ indicates that at small distance spin effects are important, even at energies as high as 12 GeV.

Since there is no satisfactory theory of the two-nucleon interaction above the pion threshold, phenomenological approaches, such as potential models, phase-shift analysis, or dispersion relations, are needed to calculate the p-p scattering amplitudes. The reliability of these methods depends both on the inherent assumptions involved and on the quality and amount of experimental data. Rarely measured complex polarization parameters are particularly important here as they provide information about the relative magnitudes and phases of individual amplitudes. However, despite some impressive successes from these methods, much uncertainty still remains in these approaches. At low energies, progress in the construction of a realistic potential by the Paris group has been made,[6] while at high energies, quark and parton models have had a good deal of success.

It was already recognized in early studies of NN scattering that hadronic interactions are complicated. The forces were seen to be strongly spin-dependent, and measurements were crucial keys to unraveling this spin structure. It is a problem of long-standing difficulty to determine the scattering matrix from polarization data in a way that is reliable, efficient, and expedient. At sufficiently low energies, where the scattering is mainly elastic, phase-shift models have been used to advantage. However, because of experimental uncertainties, gaps in data, or incomplete information, the scattering matrix is usually determined subject to both discrete and continuous ambiguities. Such ambiguities may prevent a meaningful comparison of theory with experiment. One suggestion to remove these ambiguities of phase-shift analysis was to do a sufficient number of measurements at each angle and energy for a complete reconstruction of the scattering matrix, up to an overall phase. This suggestion becomes particularly important in the inelastic region, where a large number of phase shifts can contribute. The only unambiguous method, therefore, is to perform a sufficient number of experiments (12—16) at a given angle and energy. Probably the most important factor, and one often overlooked, is the precise effect of experimental error on the determination of the amplitudes. An otherwise reasonable set of experiments may give no useful results if the level of experimental error is too large.

A polarized target and beam are needed for these measurements. In such experiments, the polarizations of the outgoing protons may or may not be observed. In the latter case, the experiment is simpler since there is no requirement for a polarimeter. We have started our program at SIN with this kind of measurement. The parameters A_{00nn} and A_{00n0} (see Sec. III for the definition) were determined by measuring the scattering asymmetry of a vertically polarized beam on a vertically polarized target for the $\theta_{\text{c.m.}}$ scattering angles 30°—90° at seven energies

between 400 and 600 MeV.[7] We report here the results of a subsequent experiment, also done at SIN, in which the cryostat of the polarized target was modified to allow a horizontal polarization axis. The solid angle in the horizontal plane was, however, restricted by the coil generating the magnetic field so that in order to observe both the recoil and scattered protons, the polarization orientation of the target was placed at angle α with respect to beam axis. Therefore, we have measured the spin-correlation parameters A_{00kk}, A_{00sk}, and A_{00ss} always as two linear combinations, namely, $(aA_{00kk}+bA_{00ks})$ and $(cA_{00sk}+dA_{00ss})$. In the first case, the beam was longitudinally polarized. For the second combination the beam was transversely polarized in the horizontal plane.

In Sec. II, we describe the experimental apparatus. Section III comprises a brief description of the formalism. The reader is referred to Ref. 8 for construction and other details not considered here. In Secs. IV–VI, we discuss the method of taking data and the analysis which produced the results presented in Sec. VII.

II. EXPERIMENTAL APPARATUS

These experiments were performed at the PM1 polarized proton-beam line at SIN using an apparatus which is very similar to the one used for our A_{00nn} measurement[7] and is sketched in Fig. 1. The technical details can be found in Ref. 8. Polarized protons were produced either by scattering off a beryllium target at 8° (scattered beam) or a polarized ion source (accelerated beam). The beam polarization in the scattered mode was $(41.65\mp1)\%$ and $\simeq(85\mp2)\%$ in the accelerated mode. A 5-T superconducting solenoid in combination with deflecting magnets was used to control the orientation of the beam polarization. Orientations along the three orthogonal directions were possible. Typical intensities used in this experiment were on the order of 10^6 protons/sec at all energies.

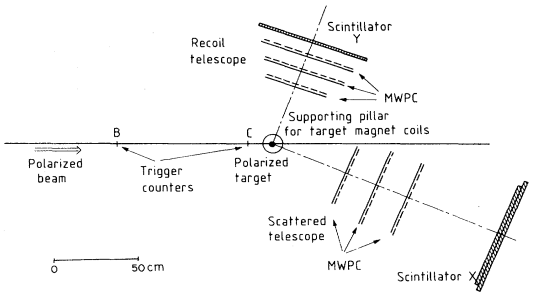

FIG. 1. The experimental setup.

A conventional butanol target polarized by dynamic nuclear orientation was used. The description of this target is given in Refs. 7–10. To obtain a polarization in the horizontal plane, the superconducting coil and target cavity were rotated by 90° into the horizontal plane and mounted into the vertical cryostat.[9] Figure 2 shows the top view of the target in this position along with trajectories of the incident and outgoing protons. The target cavity and coils could both be rotated about the vertical axis. In this arrangement, the solid angle in the horizontal plane was restricted by the superconducting coils so that the target had to be oriented at an angle with respect to the beam axis, in order to have access to the desired *p-p* scattering angular range. For this reason, we could only measure linear combinations of the desired spin-correlation parameters. Typical polarizations used in this experiment were about 60%.

The scattered and recoil protons which emerged from the target were detected by two (scattered and recoil) multiwire-proportional-chamber (MWPC) telescopes each mounted on a separate movable platform. The incident proton beam was defined by two counters *B* and *C*. These

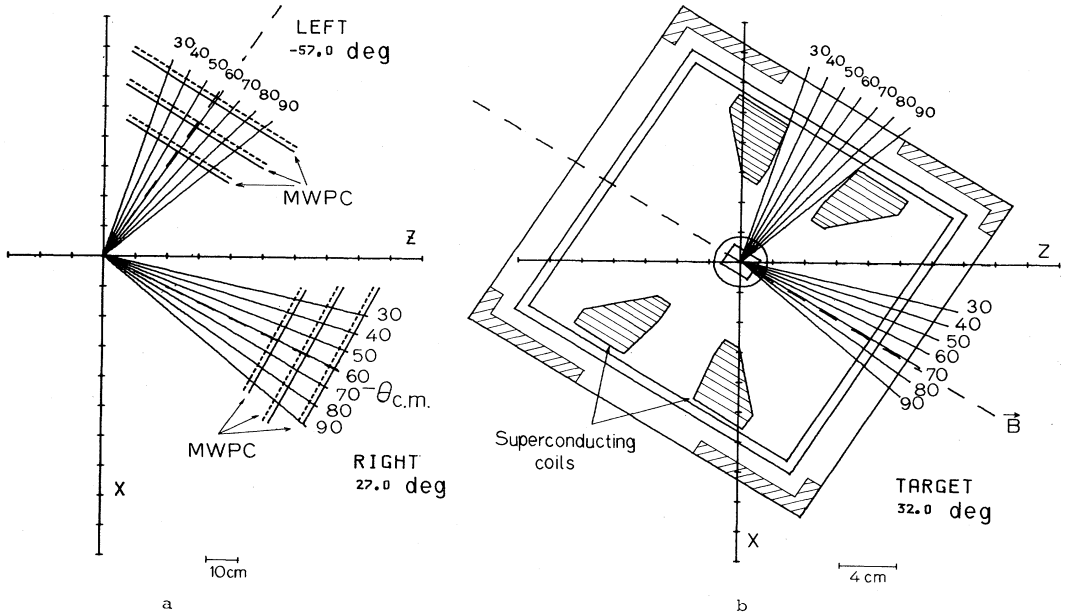

FIG. 2. (a) A top view of the trajectories for outgoing protons as seen by the MWPC's. (b) An enlarged view of the target region showing the geometrical restrictions of the superconducting coils for detecting the outgoing protons.

were small counters having dimensions 1×1 cm^2. To ensure that the proton passed directly through the polarized target, the C counter was positioned directly against the target's protective outer shell. The number of gated coincidences between B and C then gave directly the number of incident particles. The trigger was $BCXY$.

III. FORMALISM

The formalism of proton-proton scattering at medium energies has already been treated extensively in the literature and we present here only these formulas relevant to this experiment. A more detailed discussion along with further references may be found in the paper by Bystricky *et al.*,[11] whose notation we use throughout this paper.

If, in the laboratory frame of reference, we define the directions

$$\hat{k},\ \hat{n}=\hat{k}\times\hat{k}'/|\hat{k}\times\hat{k}'|,\ \hat{s}=\hat{n}\times\hat{k}\ , \tag{1}$$

where $\hat{k}$ and $\hat{k}'$ are the unit vectors in the direction of the initial and scattered particles, respectively, the differential cross section for the elastic scattering of polarized protons, $\sigma(\theta)$, can be written as

$$\sigma(\theta)=\sigma_0(\theta)[1+P(\theta)(\vec{P}_b\cdot\hat{n}+\vec{P}_t\cdot\hat{n})+\vec{P}_b\cdot\hat{n}\,\vec{P}_t\cdot\hat{n}\,A_{00nn}(\theta)+\vec{P}_b\cdot\hat{s}\,\vec{P}_t\cdot\hat{s}\,A_{00ss}(\theta)$$
$$+(\vec{P}_b\cdot\hat{s}\,\vec{P}_t\cdot\hat{k}+\vec{P}_b\cdot\hat{k}\,\vec{P}_t\cdot\hat{s})A_{00sk}(\theta)+\vec{P}_b\cdot\hat{k}\,\vec{P}_t\cdot\hat{k}\,A_{00kk}(\theta)]\ , \tag{2}$$

where $\vec{P}_b$ and $\vec{P}_t$ are the beam and target polarization and we have used the relations $A_{00ks}=A_{00sk}$ and $A_{00n0}=A_{000n}=P$. P is the polarization parameter and A_{00ij} is the correlation parameter between i and j components of spin and $\sigma_0(\theta)$ the elastic differential cross section for unpolarized protons. All quantities are expressed as functions of the c.m. scattering angle θ. Expression (2) can be rewritten as

$$\sigma(\theta)=\sigma_0(\theta)[1+P(\theta)(P_bf_{n0}+P_tf_{0n})+P_bP_tA_{pq}(\theta)] \tag{3}$$

with

$$A_{pq}(\theta)=f_{nn}A_{00nn}(\theta)+f_{ss}A_{00ss}(\theta)$$
$$+(f_{sk}+f_{ks})A_{00ks}(\theta)+f_{kk}A_{00kk}(\theta)\ , \tag{4}$$

where f_{ij} are the coefficients defined by

$$f_{ij}=(\vec{P}_b\cdot\hat{i}/|\vec{P}_b|)(\vec{P}_t\cdot\hat{j}/|\vec{P}_t|)\ . \tag{5}$$

Because of the magnetic field of the target, the $\hat{k}$ direction is no longer in the horizontal plane at the center of the target. At this point, one can define new x,y,z axes such that

$$\hat{z}=\hat{k}\ ,$$
$$\hat{x}=\text{horizontal and perpendicular to }\hat{z}\ , \tag{6}$$
$$\hat{y}=\hat{z}\times\hat{x}$$

Then we can define the azimuthal scattering angle ϕ as

$$\cos\phi=\hat{n}\cdot\hat{y},\ \sin\phi=-\hat{n}\cdot\hat{x}\ . \tag{7}$$

Figure 3 shows an example of the positions of the final-particle trajectories in our last MWPC of each arm for various θ and ϕ angles. Here one can see the "turning" effect of the magnetic field.

In terms of the $\hat{x},\hat{y},\hat{z}$ axes, the s,n,k directions are

$$\hat{s}=\hat{x}\cos\phi+\hat{y}\sin\phi\ ,$$
$$\hat{n}=-\hat{x}\sin\phi+\hat{y}\cos\phi\ ,\ \hat{k}=\hat{z}\ . \tag{8}$$

If $\vec{P}_b$ and $\vec{P}_t$ are now referred to the x,y,z axes, then f_{ij} are functions of ϕ expressed as

$$f_{0n}(\phi)=(P_{by}/P_b)\cos\phi-(P_{bx}/P_b)\sin\phi\ ,$$
$$f_{n0}(\phi)=(P_{ty}/P_t)\cos\phi-(P_{tx}/P_t)\sin\phi\ ,$$
$$f_{nn}(\phi)=(P_{by}P_{ty}/P_bP_t)\cos^2\phi+(P_{bx}P_{tx}/P_bP_t)\sin^2\phi-(P_{by}P_{tx}/P_bP_t+P_{bx}P_{ty}/P_bP_t)\sin\phi\cos\phi\ ,$$
$$f_{ss}(\phi)=(P_{by}P_{ty}/P_bP_t)\sin^2\phi+(P_{bx}P_{tx}/P_bP_t)\cos^2\phi+(P_{by}P_{tx}/P_bP_t+P_{bx}P_{ty}/P_bP_t)\sin\phi\cos\phi\ , \tag{9}$$
$$f_{sk}(\phi)+f_{ks}(\phi)=(P_{by}P_{tz}/P_bP_t+P_{ty}P_{bz}/P_tP_b)\sin\phi+(P_{bx}P_{tz}/P_bP_t+P_{tx}P_{bz}/P_tP_b)\cos\phi\ ,$$
$$f_{kk}=P_{bz}P_{tz}/P_bP_t\ .$$

By using Eq. (3), the experimental event rate for each P_b and P_t configuration can be expressed as

$$N_{P_bP_t}(\theta,\phi)=\sigma_0(\theta)G(\theta,\phi)\{1+P(\theta)[P_bf_{0n}(\phi)+P_tf_{n0}(\phi)]+P_bP_tA_{pq}(\theta,\phi)\}\ , \tag{10}$$

where $G(\theta,\phi)$ is the acceptance function which takes into account the geometrical acceptance of the measuring apparatus, losses due to particle absorption, etc.

In this experiment, events were integrated over a finite ϕ range $(\phi_{\min},\phi_{\max})$ where the acceptance $G(\theta,\phi)$ was found to be independent of ϕ. Equation (10) then becomes

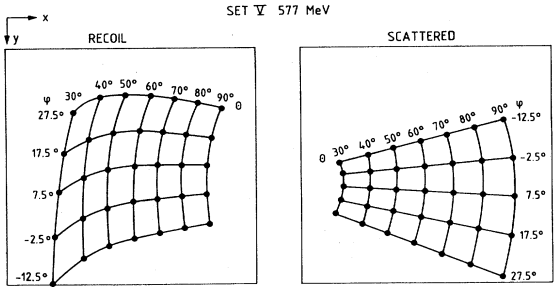

FIG. 3. An example of the positions of the final-particle trajectories in our detectors for various θ and ϕ angles.

$$N_{P_bP_t}(\theta)=\sigma_0(\theta)\bar{G}(\theta)[1+P(\theta)(P_b\bar{f}_{0n}+P_t\bar{f}_{n0}) +P_bP_t\bar{A}_{pq}(\theta)] , \quad (11)$$

where

$$\bar{A}_{pq}(\theta)=\bar{f}_{nn}A_{00nn}(\theta)+\bar{f}_{ss}A_{00ss}(\theta) +(\bar{f}_{sk}+\bar{f}_{ks})A_{00ks}(\theta)+\bar{f}_{kk}A_{00kk}(\theta) . \quad (12)$$

Values of $\phi_{\min}$, $\phi_{\max}$, $\alpha_{\text{beam-target}}$, P_b and P_t components, and the consequent f_{ij} depend on the particular experimental geometry. These are given in Tables I and II.

If $N_{P_bP_t}(\theta)$ is measured for various beam-target polarization orientations, i.e., $(P_b,P_t)=(-,+)$, $(-,-)$, $(-,0)$, $(+,+)$, $(+,-)$, and $(+,0)$, one obtains a set of six equations from which the parameter A_{pq} can be calculated.

IV. EVENT RECONSTRUCTION

Data were reconstructed using a fast on-line event-reconstruction technique.[7,10] The reader is referred to Ref. 12 for the details not considered here. This method, based on a simplification of the reconstruction equations by a linearization method, essentially sacrifices some reconstruction accuracy for a much larger gain in execution speed.

If one considers a detection system such as we have described where the coordinates of the final-state particle trajectories are measured, for each scattering event, there exists a unique set of coordination which corresponds to the set of scattering parameters characterizing the event, i.e., scattering angle, interaction vertex, etc. If we express these scattering parameters as a vector p and the coordinates as another vector x, we can write

$$x=F(p) , \quad (13)$$

where F is the functional relation between p and x.

The reconstruction of p for a scattering event with set of measured coordinates x, then, involves an evaluation of the inverse relation

$$p=F^{-1}(x) . \quad (14)$$

The linearization technique consists of approximating F by the first-order expansion

$$x=F(p_0)+\partial F/\partial p\,|_{p_0}(p-p_0)=x_0+L(p-p_0) , \quad (15)$$

where p_0 is some fixed central point, x_0 $[=F(p_0)]$ is the corresponding central coordinate, and L is the matrix of first derivatives of F evaluated at p_0.

To reconstruct p from given x, we invert Eq. (15) by using the method of least-squares fit,

$$p-p_0=(L^TL)^{-1}L^T(x-x_0)=R(x-x_0) , \quad (16)$$

where $R=(L^TL)^{-1}L^T$. Event reconstruction is thus reduced to a fast and a simple matrix multiplication. The R matrices were generated off line prior to the experiment with the help of a conventional tracking program. Five scattering parameters $\theta_{\text{c.m.}}$, ϕ, and the scattering-vertex coordinates (x,y,z) were reconstructed from the 12 X-Y MWPC readouts of the final-state telescopes. As a test of the quality of reconstruction, a χ^2 parameter was calculated for each event accepted by this program.

$$S^2=[x(\text{measured})-x(\text{theoretical})] \cdot[x(\text{meas})-x(\text{theor})]/\nu , \quad (17)$$

where ν is the number of degrees of freedom and x(theor) was found by using the inverse of the reconstruction matrix L.

To check the accuracy of the reconstruction, chamber coordinates for known sets of scattering parameters were generated using a tracking program. These coordinates were then fed into the matrix reconstruction program and the results compared to the known parameters. Such a procedure estimated the nonlinearity of the true reconstruction function F. For the first half of the data in this experiment, these nonlinearities could only be corrected off line using the method described in Ref. 7. These nonlinearity corrections required a readjustment of the bin limits in θ and ϕ, thus resulting in a slightly different value for the central-bin value (method A).

Towards the latter half of the experiment, the on-line reconstruction program was modified so as to allow the reconstructed parameters to be corrected directly for each event. This was performed using a correction table generated as a function of the reconstructed $\theta_{\text{c.m.}}$ and ϕ. The table was loaded into the computer memory and the corrections "looked up" after each event passed through the matrix multiplication in Eq. (16) (method B).

A further improvement to this matrix procedure can be made by including a covariance matrix C taking into account the finite resolution of the detectors in Eq. (16). In such a case the reconstruction matrix becomes

$$R=(L^TCL)^{-1}L^TC . \quad (18)$$

TABLE I. Summary of the data sets taken in this experiment.

Energy (MeV)	Set number	Beam-target angle α (deg)	Range in $\theta_{c.m.}$ (deg) $\theta_0 \pm \Delta\theta$	Range in ϕ (deg) $\phi_0 \pm \Delta\phi$	P_{bx}/P_b	P_{by}/P_b	P_{bz}/P_b	P_{tx}/P_t	P_{ty}/P_t	P_{tz}/P_t	Reconstruction method	Reconstruction mode
577	I	78.5	45±20	177.5±22.5	0.002	0.131	0.991	0.980	−0.009	0.200	A	On-line
	II	32	60±32	7.5±22.5	0.001	0.067	0.998	0.530	−0.019	0.848	A	On-line
	III	101.5	44±16	−5 ±20	1.000	0.002	0.003	0.980	0.009	−0.200	B	On-line
	IV	−8	76±32	5 ±20	0.974	−0.225	−0.003	−0.139	0.006	0.990	B	On-line
	V	32	60±32	7.5±20	0.975	−0.223	0.012	0.530	−0.019	0.848	B	Off-line
536	I	78.5	45±20	177.5±22.5	0.044	0.133	0.990	0.980	−0.009	0.200	A	On-line
	II	32	60±32	7.5±22.5	0.042	0.058	0.997	0.530	−0.020	0.848	A	On-line
	IV	−8	76±16	5 ±20	0.972	−0.235	−0.003	−0.139	0.006	0.990	B	On-line
	V	32	60±32	7.5±20	0.972	−0.223	0.013	0.530	−0.020	0.848	B	On-line
514	I	78.5	45±20	177.5±22.5	0.066	0.134	0.989	0.980	−0.010	0.200	A	On-line
	II	32	60±32	7.5±22.5	0.064	0.053	0.997	0.530	−0.021	0.848	A	On-line
	III	101.5	44±16	−5 ±20	1.000	0.002	0.003	0.980	0.010	−0.200	B	On-line
	IV	−8	76±32	5 ±20	0.971	−0.241	−0.003	−0.139	0.006	0.990	B	On-line
	V	32	60±32	7.5±20	0.971	−0.239	0.013	0.530	−0.021	0.848	B	Off-line
494	I	78.5	45±20	177.5±22.5	0.088	0.135	0.987	0.980	−0.010	0.200	A	On-line
	II	32	60±32	7.5±22.5	0.084	0.048	0.995	0.530	−0.021	0.848	A	On-line
	IV	−8	76±16	5 ±20	0.969	−0.247	−0.003	−0.139	0.006	0.990	B	On-line
	V	32	60±32	7.5±20	0.969	−0.245	0.014	0.530	−0.021	0.848	B	On-line and off-line
445	I	78.5	45±20	177.5±22.5	0.138	0.138	0.981	0.980	−0.011	0.200	A	On-line
	II	32	60±32	7.5±22.5	0.133	0.036	0.991	0.530	−0.023	0.848	A	On-line
	IV	−8	76±16	5 ±20	0.965	−0.262	−0.003	−0.139	0.006	0.990	B	On-line
	V	32	60±32	7.5±20	0.965	−0.260	0.015	0.530	−0.023	0.848	B	On-line
	VI	32	52±24	3 ±15	0.132	0.036	0.991	0.530	−0.023	0.848	C	Off-line with on-line filter
	VII	32	52±24	3 ±15	0.966	−0.260	0.015	0.530	−0.023	0.848	C	Off-line with on-line filter
	VIII	101.5	44±16	−5 ±15	0.123	0.139	0.982	0.980	0.011	−0.200	C	Off-line with on-line filter
	IX	101.5	44±16	−5 ±15	0.999	0.002	0.004	0.980	0.011	−0.200	C	Off-line with on-line filter

TABLE II. Measured values of A_{pq} at 577, 536, 514, 494, and 445 MeV.

577 MeV (±3)														
Set I $\Delta A_{pq}/A_{pq}=0.10$[a]			Set II $\Delta A_{pq}/A_{pq}=0.10$[a]			Set III $\Delta A_{pq}/A_{pq}=0.06$[a]			Set IV $\Delta A_{pq}/A_{pq}=0.06$[a]			Set V $\Delta A_{pq}/A_{pq}=0.07$[a]		
$\theta_{c.m.}$ (deg)	A_{pq}	σ[b]	$\theta_{c.m.}$ (deg)	A_{pq}	σ[b]	$\theta_{c.m.}$ (deg)	A_{pq}	σ[b]	$\theta_{c.m.}$ (deg)	A_{pq}	σ[b]	$\theta_{c.m.}$ (deg)	A_{pq}	σ[b]
36.36	0.252	0.021	38.64	0.252	0.017	30	−0.218	0.014				30	−0.281	0.031
41.13	0.219	0.019	41.84	0.245	0.017	34	−0.254	0.010	54	0.011	0.021	34	−0.311	0.020
46.09	0.161	0.020	45.91	0.238	0.017	38	−0.287	0.009	58	0.036	0.016	38	−0.303	0.016
51.21	0.153	0.020	49.88	0.237	0.016	42	−0.296	0.009	62	0.039	0.015	42	−0.304	0.014
56.33	0.135	0.020	53.90	0.223	0.016	46	−0.329	0.009	66	0.047	0.015	46	−0.290	0.013
61.32	0.132	0.021	57.93	0.229	0.016	50	−0.337	0.009	70	0.051	0.015	50	−0.280	0.013
			61.96	0.233	0.017	54	−0.355	0.014	74	0.047	0.015	54	−0.305	0.013
			66.00	0.201	0.017	58	−0.408	0.125	78	0.069	0.016	58	−0.252	0.013
			70.04	0.188	0.017				82	0.091	0.017	62	−0.266	0.013
			74.01	0.162	0.018				86	0.062	0.017	66	−0.253	0.013
			77.94	0.194	0.019				90	0.119	0.018	70	−0.263	0.013
			81.88	0.141	0.020				94	0.089	0.022	74	−0.240	0.013
			85.66	0.171	0.021							78	−0.249	0.013
			89.89	0.173	0.022							82	−0.251	0.013
												86	−0.264	0.014
												90	−0.230	0.016

Set I $A_{pq}=0.007A_{nn}-0.006A_{ss}-0.944A_{sk}+0.198A_{kk}$
Set II $A_{pq}=-0.006A_{nn}+0.006A_{ss}+0.517A_{sk}+0.846A_{kk}$
Set III $A_{pq}=0.045A_{nn}+0.935A_{ss}-0.192A_{sk}-0.001A_{kk}$
Set IV $A_{pq}=-0.010A_{nn}-0.127A_{ss}+0.923A_{sk}-0.003A_{kk}$
Set V $A_{pq}=0.049A_{nn}+0.473A_{ss}+0.783A_{sk}+0.010A_{kk}$

TABLE II. *(Continued.)*

536 MeV (±3)

Set I $\Delta A_{pq}/A_{pq}=0.06$[a]			Set II $\Delta A_{pq}/A_{pq}=0.06$[a]			Set IV $\Delta A_{pq}/A_{pq}=0.06$[a]			Set V $\Delta A_{pq}/A_{pq}=0.06$[a]		
$\theta_{c.m.}$ (deg)	A_{pq}	σ[b]	$\theta_{c.m.}$ (deg)	A_{pq}	σ[b]	$\theta_{c.m.}$ (deg)	A_{pq}	σ[b]	$\theta_{c.m.}$ (deg)	A_{pq}	σ[b]
36.39	0.261	0.020	37.46	0.245	0.025						
41.23	0.254	0.018	41.95	0.242	0.024	62	−0.027	0.016	34	−0.309	0.026
46.23	0.248	0.018	45.85	0.250	0.023	66	0.010	0.016	38	−0.310	0.021
51.30	0.213	0.018	49.88	0.221	0.023	70	0.004	0.017	42	−0.290	0.020
56.37	0.154	0.017	53.90	0.237	0.023	74	0.017	0.017	46	−0.314	0.020
61.37	0.086	0.018	57.94	0.226	0.023	78	0.054	0.017	50	−0.296	0.021
			61.99	0.217	0.023	82	0.036	0.018	54	−0.286	0.022
			66.04	0.169	0.023	86	0.042	0.018	58	−0.293	0.023
			70.06	0.177	0.023	90	0.079	0.019	62	−0.341	0.024
			74.06	0.138	0.024				66	−0.268	0.024
			78.00	0.139	0.025				70	−0.286	0.024
			81.91	0.068	0.026				74	−0.259	0.025
			85.78	0.112	0.028				78	−0.284	0.025
			89.63	0.144	0.029				82	−0.286	0.025
									86	−0.284	0.026
									90	−0.284	0.027

Set I $A_{pq}=0.009A_{nn}+0.033A_{ss}-0.952A_{sk}+0.198A_{kk}$
Set II $A_{pq}=-0.004A_{nn}+0.025A_{ss}+0.547A_{sk}+0.845A_{kk}$
Set IV $A_{pq}=-0.010A_{nn}-0.126A_{ss}+0.920A_{sk}-0.003A_{kk}$
Set V $A_{pq}=0.050A_{nn}+0.471A_{ss}+0.781A_{sk}+0.011A_{kk}$

TABLE II. *(Continued.)*

514 MeV (±3)

Set I $\Delta A_{pq}/A_{pq}=0.06$[a]			Set II $\Delta A_{pq}/A_{pq}=0.06$[a]			Set III $\Delta A_{pq}/A_{pq}=0.09$[a]			Set IV $\Delta A_{pq}/A_{pq}=0.06$[a]			Set V $\Delta A_{pq}/A_{pq}=0.08$[a]		
$\theta_{c.m.}$ (deg)	A_{pq}	σ[b]	$\theta_{c.m.}$ (deg)	A_{pq}	σ[b]	$\theta_{c.m.}$ (deg)	A_{pq}	σ[b]	$\theta_{c.m.}$ (deg)	A_{pq}	σ[b]	$\theta_{c.m.}$ (deg)	A_{pq}	σ[b]
36.51	0.320	0.022	38.49	0.264	0.023	30	−0.234	0.023						
41.26	0.276	0.019	41.89	0.255	0.021	34	−0.221	0.011	54	−0.063	0.022	34	−0.315	0.019
46.25	0.260	0.019	45.92	0.289	0.020	38	−0.242	0.009	58	−0.060	0.015	38	−0.341	0.015
51.32	0.226	0.019	49.92	0.265	0.020	42	−0.275	0.008	62	−0.032	0.014	42	−0.336	0.013
56.39	0.145	0.019	53.94	0.203	0.020	46	−0.303	0.008	66	0.010	0.014	46	−0.331	0.012
61.38	0.159	0.020	57.97	0.224	0.019	50	−0.343	0.008	70	−0.007	0.014	50	−0.316	0.012
			62.02	0.143	0.019	54	−0.356	0.010	74	0.026	0.014	54	−0.307	0.012
			66.07	0.175	0.019	58	−0.431	0.044	78	0.032	0.015	58	−0.301	0.012
			70.08	0.130	0.020				82	0.041	0.015	62	−0.318	0.012
			74.07	0.155	0.020				86	0.067	0.016	66	−0.288	0.012
			78.03	0.088	0.021				90	0.055	0.017	70	−0.294	0.012
			81.91	0.058	0.022				94	0.069	0.023	74	−0.306	0.013
			85.83	0.107	0.023							78	−0.289	0.012
			89.29	0.098	0.024							82	−0.310	0.013
												86	−0.273	0.013
												88.2	−0.262	0.014

Set I $A_{pq}=0.011A_{nn}+0.054A_{ss}-0.955A_{sk}+0.197A_{kk}$
Set II $A_{pq}=-0.002A_{nn}+0.035A_{ss}+0.562A_{sk}+0.845_{kk}$
Set III $A_{pq}=0.045A_{nn}+0.935A_{ss}-0.192A_{sk}-0.001A_{kk}$
Set IV $A_{pq}=-0.010A_{nn}-0.126A_{ss}+0.921A_{sk}-0.003A_{kk}$
Set V $A_{pq}=0.051A_{nn}+0.469A_{ss}+0.778A_{sk}+0.011A_{kk}$

TABLE II. *(Continued.)*

494 MeV (±3)													
Set I $\Delta A_{pq}/A_{pq}=0.06$[a]			Set II $\Delta A_{pq}/A_{pq}=0.06$[a]			Set IV $\Delta A_{pq}/A_{pq}=0.06$[a]			Set V (scattered) $\Delta A_{pq}/A_{pq}=0.06$[a]			Set V (accelerated) $\Delta A_{pq}/A_{pq}=0.07$[a]	
$\theta_{c.m.}$ (deg)	A_{pq}	σ[b]	$\theta_{c.m.}$ (deg)	A_{pq}	σ[b]	$\theta_{c.m.}$ (deg)	A_{pq}	σ[b]	$\theta_{c.m.}$ (deg)	A_{pq}	σ[b]	$\theta_{c.m.}$ (deg)	A_{pq}	σ[b]
36.74	0.330	0.026	38.04	0.322	0.024									
41.30	0.350	0.021	41.99	0.318	0.022	62	−0.001	0.022	34	−0.404	0.036	34	−0.433	0.036
46.28	0.281	0.020	45.96	0.316	0.021	66	−0.008	0.021	38	−0.348	0.024	38	−0.330	0.027
51.34	0.224	0.020	49.96	0.317	0.021	70	0.027	0.022	42	−0.355	0.021	42	−0.388	0.023
56.41	0.188	0.020	53.98	0.283	0.021	74	0.029	0.022	46	−0.338	0.021	46	−0.364	0.022
61.41	0.171	0.021	58.01	0.292	0.021	78	0.081	0.022	50	−0.345	0.021	50	−0.366	0.022
			62.05	0.246	0.020	82	0.084	0.022	54	−0.335	0.022	54	−0.347	0.021
			66.09	0.229	0.020	86	0.063	0.022	58	−0.322	0.022	58	−0.342	0.021
			70.11	0.205	0.021	90	0.106	0.022	62	−0.320	0.023	62	−0.314	0.022
			74.08	0.168	0.022				66	−0.342	0.023	66	−0.335	0.021
			78.02	0.131	0.023				70	−0.351	0.024	70	−0.322	0.022
			81.95	0.129	0.023				74	−0.352	0.024	74	−0.302	0.022
			85.72	0.118	0.024				78	−0.334	0.024	78	−0.282	0.021
			89.95	0.108	0.026				82	−0.291	0.024	82	−0.295	0.022
									86	−0.321	0.025	86	−0.308	0.022
									90	−0.310	0.027	90	−0.269	0.025

Set I $A_{pq}=0.011A_{nn}+0.074A_{ss}-0.958A_{sk}+0.197A_{kk}$
Set II $A_{pq}=-0.001A_{nn}+0.045A_{ss}+0.579A_{sk}+0.844A_{kk}$
Set IV $A_{pq}=-0.010A_{nn}-0.126A_{ss}+0.916A_{sk}-0.003A_{kk}$
Set V $A_{pq}=0.051A_{nn}+0.467A_{ss}+0.777A_{sk}+0.012A_{kk}$

TABLE II. *(Continued.)*

445 MeV (±3)

Set I $\Delta A_{pq}/A_{pq}=0.06$[a]			Set II $\Delta A_{pq}/A_{pq}=0.06$[a]			Set IV $\Delta A_{pq}/A_{pq}=0.06$[a]			Set V $\Delta A_{pq}/A_{pq}=0.06$[a]		
$\theta_{c.m.}$ (deg)	A_{pq}	σ[b]	$\theta_{c.m.}$ (deg)	A_{pq}	σ[b]	$\theta_{c.m.}$ (deg)	A_{pq}	σ[b]	$\theta_{c.m.}$ (deg)	A_{pq}	σ[b]
36.83	0.252	0.026	37.78	0.235	0.026				34	−0.411	0.036
41.35	0.311	0.019	42.01	0.249	0.023	62	−0.063	0.019	38	−0.350	0.027
46.36	0.269	0.019	45.96	0.320	0.022	66	−0.037	0.018	42	−0.336	0.024
51.43	0.196	0.019	49.95	0.257	0.021	70	0.005	0.019	46	−0.313	0.022
56.48	0.134	0.019	53.96	0.249	0.021	74	−0.014	0.018	50	−0.328	0.022
61.47	0.088	0.020	58.02	0.238	0.020	78	0.075	0.019	54	−0.356	0.022
			62.07	0.184	0.020	82	0.043	0.019	58	−0.299	0.022
			66.11	0.119	0.020	86	0.063	0.019	62	−0.294	0.024
			70.13	0.154	0.020	90	0.098	0.020	66	−0.300	0.024
			74.11	0.135	0.021				70	−0.298	0.024
			78.06	0.117	0.022				74	−0.278	0.025
			82.01	0.101	0.022				78	−0.326	0.025
			85.73	0.054	0.023				82	−0.291	0.025
			90.34	0.066	0.025				86	−0.306	0.025
									90	−0.268	0.028

Set I $A_{pq}=0.014A_{nn}+0.120A_{ss}-0.962A_{sk}+0.196A_{kk}$
Set II $A_{pq}=0.002A_{nn}+0.067A_{ss}+0.614A_{sk}+0.840A_{kk}$
Set IV $A_{pq}=-0.010A_{nn}-0.126A_{ss}+0.911A_{sk}-0.003A_{kk}$
Set V $A_{pq}=0.053A_{nn}+0.464A_{ss}+0.772A_{sk}+0.013A_{kk}$

TABLE II. *(Continued.)*

445 MeV (±3)

Set VI $\Delta A_{pq}/A_{pq}=0.05$[a]			Set VII $\Delta A_{pq}/A_{pq}=0.05$[a]			Set VIII $\Delta A_{pq}/A_{pq}=0.05$[a]			Set IX $\Delta A_{pq}/A_{pq}=0.05$[a]		
$\theta_{c.m.}$ (deg)	A_{pq}	σ[b]	$\theta_{c.m.}$ (deg)	A_{pq}	σ[b]	$\theta_{c.m.}$ (deg)	A_{pq}	σ[b]	$\theta_{c.m.}$ (deg)	A_{pq}	σ[b]
34	0.127	0.057	34	−0.400	0.047	30	−0.393	0.057	30	−0.240	0.084
38	0.258	0.039	38	−0.374	0.034	34	−0.439	0.020	34	−0.279	0.029
42	0.224	0.033	42	−0.376	0.032	38	−0.393	0.013	38	−0.324	0.020
46	0.326	0.031	46	−0.405	0.033	42	−0.365	0.013	42	−0.364	0.019
50	0.205	0.029	50	−0.352	0.033	46	−0.335	0.012	46	−0.404	0.018
54	0.248	0.029	54	−0.390	0.033	50	−0.320	0.012	50	−0.430	0.017
58	0.244	0.028	58	−0.385	0.034	54	−0.282	0.012	54	−0.450	0.017
62	0.246	0.028	62	−0.336	0.034	58	−0.289	0.178			
66	0.206	0.027	66	−0.385	0.034						
70	0.151	0.028	70	−0.347	0.035						
			74	−0.354	0.047						

Set VI $A_{pq}=-0.0002A_{nn}+0.0690A_{ss}+0.6280A_{sk}+0.8400A_{kk}$
Set VII $A_{pq}=+0.0160A_{nn}+0.5022A_{ss}+0.8115A_{sk}+0.0120A_{kk}$
Set VIII $A_{pq}=+0.0169A_{nn}+0.1060A_{ss}+0.9240A_{sk}-0.1960A_{kk}$
Set IX $A_{pq}=+0.0300A_{nn}+0.9490A_{ss}-0.1930A_{sk}-0.0010A_{kk}$

[a]Systematic errors to be added quadratically.
[b]Errors are purely statistical.

The χ^2 definition is thus improved and becomes

$$\chi^2=[x(\text{meas})-x(\text{theor})]^T \times C[x(\text{meas})-x(\text{theor})]/\nu \ . \quad (19)$$

This was used only in the last set of measurements (sets VI, VII, VIII, and IX at 445 MeV) and is described in more detail in Ref. 12 (method C).

Within this program it was possible to make cuts on the reconstructed parameters. As each parameter of p was reconstructed in order, the program would test to see if the calculated value fell within the range defined by the cuts. If not, the event was rejected without further processing. Events which passed all the software cuts were accumulated in a three-dimensional histogram of $\theta_{\text{c.m.}}$, ϕ, and S in the computer memory. In addition, the distributions for the other reconstructed parameters, that is, interaction vertex (x_v,y_v,z_v), were also saved and could be accessed during a data run as a check of system operation.

This technique could be used either as a true on-line reconstruction program or as an event filter. Most of the data reported here were taken in the former mode ($A+B$ in Table I). The contents of the parameter histograms accumulated at the end of each run were written onto magnetic tape and further analyzed off line in this form. Since the raw data on the detection coordinates is lost in such a procedure, a careful determination of the cuts applied on the parameters during data acquisition had to be made beforehand. However, a small part of the data (C in Table I) were taken using this method as an event filter. Here only loose cuts were imposed on the reconstructed parameters during acquisition. The raw coordinate data of events which passed these cuts were then rewritten onto magnetic tape. These events were then reconstructed again off line using the same method but with more stringent cuts. The resulting data were analyzed in a similar manner. The method of reconstruction used for each set is summarized in Table I.

V. DATA ACQUISITION

Measurements were made at five different energies 445, 494, 514, 536, and 577 MeV. These values were measured to within ± 2 MeV accuracy. Beam spread was typically ± 3 MeV. Firstly we used a longitudinally polarized beam and obtained sets I and II. Secondly, with a transversely polarized beam, we obtained the sets III, IV, and V. Since phase-shift analyses had difficulties with fitting the preliminary results of certain spin-correlation parameters at 445 MeV (Ref. 13) (see Sec. VII), these data were supplemented by further measurements which were sets VI, VII, VIII, and IX (see Table I).

For each energy, data were taken for the four beam-target configurations and also for the beam orientations with unpolarized target. The accelerated beam was only used for set V at 577, 514, and 494 MeV.

For the scattered beam, all possible target configurations were taken before changing the beam orientation to avoid changes in the system acceptance due to beam shifts and focusing effects from the solenoid. Moreover, after each change of solenoid current, the beam was carefully recentered on the target.

To account for background reactions due to the carbon and helium-3 nuclei in the butanol target, data were also taken with a dummy consisting of carbon and helium-3 alone where the total number of carbon used was determined by the constraint that the ratio of carbon nuclei to helium-3 nuclei be the same as that in the butanol target.

VI. DATA ANALYSIS

During the off-line analysis each run was corrected for background contamination, chamber efficiency, and normalized to the number of incident particles, before a determination of A_{pq} was made.

A. Chamber efficiency

The efficiency of the chamber telescopes was monitored during each run. This consisted of recording the inefficiency of the chamber planes for each accepted event; i.e., for each chamber plane, the number of times there were none or more than one spark. If one plane was inefficient in one of the telescopes, the missing coordinate was calculated by using the information of the other two chambers before entering in the reconstruction procedure (see Sec. IV). In addition, this was recorded in a histogram as a function of the reconstructed $\theta_{\text{c.m.}}$ for each event. The total efficiency could then be extracted from this information.[8,10] This was found to be very high with values not less than 97%.

B. Background subtraction

Background could be subtracted by normalizing the dummy target runs for the difference in the number of carbon atoms and the number of incident protons. However, because of other possible variations between runs, for example, system acceptance, this normalization factor was found by assuming the S distribution for each butanol run could be described by a χ^2 distribution, plus an additional term for background:

$$S^2(\text{butanol})=Q(x^2,\nu)+\beta s^2(\text{dummy}) \ , \quad (20)$$

where $Q(x^2,\nu)$ is the expression for a χ^2 distribution with ν degrees of freedom and β is the normalization factor.

Equation (20) was then fitted to the observed S^2 (butanol) distribution to obtain the normalization β. Values of β found by this method agreed quite well with the simple scaling of incident rates and the number of atoms in the butanol and dummy target, indicating no large variations of system acceptance between runs. Typical values for the background contamination were found to be between 6% and 16% depending on the polarization orientation and the geometrical acceptance.

C. Extraction of A_{pq}

A_{pq} was determined by a direct solution of the four polarized-target runs, namely, $(+,+)$, $(+,-)$, $(-,-)$, and $(-,+)$. Where unpolarized-target data $[(+,0),(-,0)]$ were available the parameters were extracted by a fitting procedure instead and the results checked by a solution of the equations. In the fitting method the equations were weighted by the measured errors and fitted for $\sigma_0\bar{G}A_{pq}$, $\sigma_0\bar{G}$, $\sigma_0\bar{G}f_{n0}P$, and $\sigma_0\bar{G}f_{0n}P$ using the usual

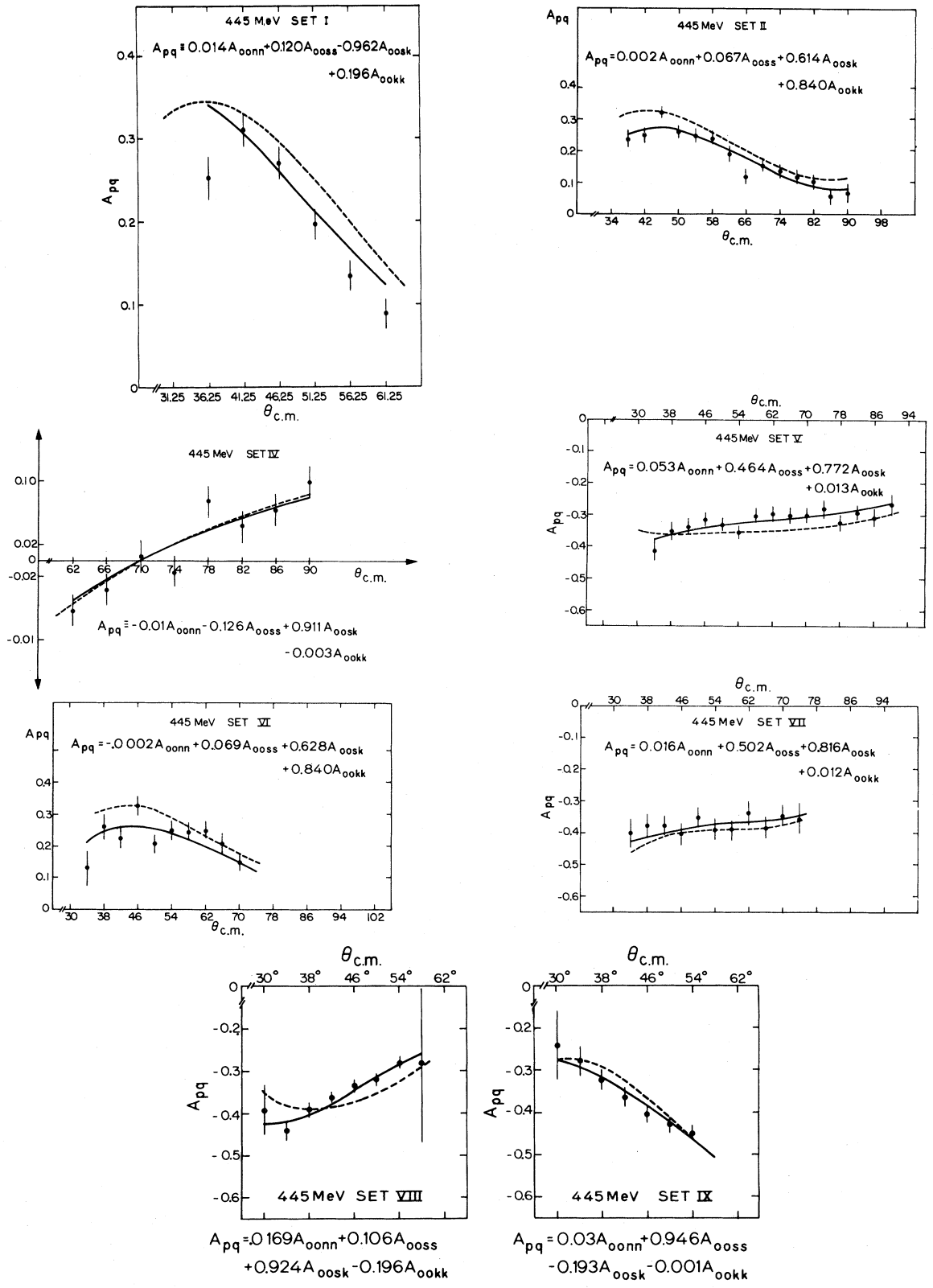

FIG. 4. A_{pq} vs $\theta_{c.m.}$ at 445 MeV for data sets I, II, IV, V, VI, VII, VIII, and IX. Points from this experimental are shown as ●. The dashed curves represent the Saclay-Geneva phase-shift predictions (Ref. 14). The solid curves are the results of the Saclay-Geneva phase-shift analysis after admission of the data from this experiment.

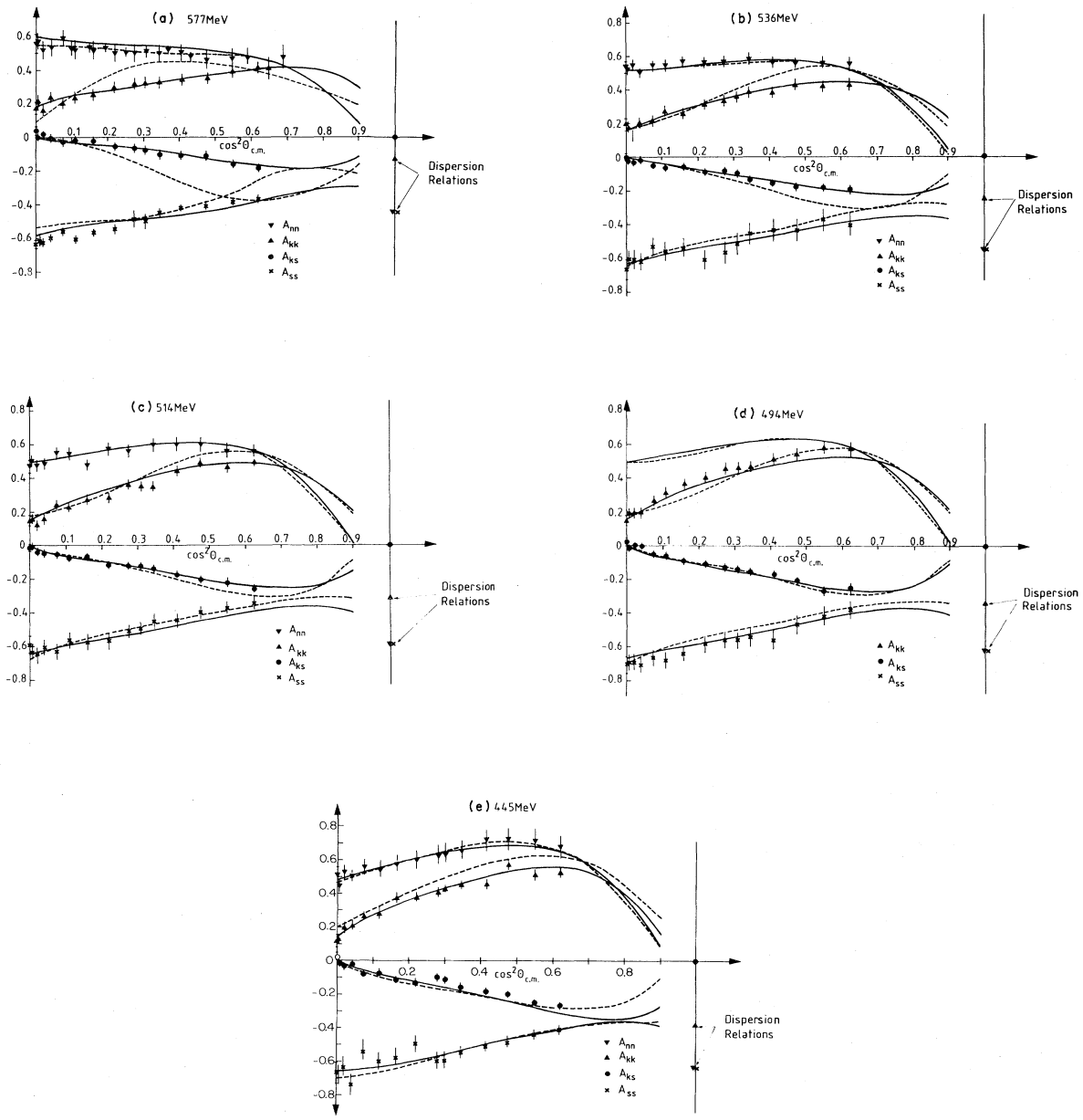

FIG. 5. (a)—(e) A_{00nn}, A_{00ss}, A_{00sk}, and A_{00kk} as a function of $\cos^2\theta_{\text{c.m.}}$ at 577, 536, 514, 494, and 445 MeV. Points from this experiment are shown as $A_{nn}=\blacktriangledown$, $A_{kk}=\blacktriangle$, $A_{ks}=\bullet$, and $A_{ss}=\times$. The dashed curves represent the Saclay-Geneva phase-shift predictions (Ref. 14). The solid curves are the results of the Saclay-Geneva phase-shift analysis after admission of the data from this experiment. Dispersion-relation calculations are from Ref. 25.

least-squares method. The data were grouped in $\theta_{\text{c.m.}}$ bins of 4° each and were fitted independently for each angle. The central values for each bin were estimated by weighting $\theta_{\text{c.m.}}$ with an acceptance density function calculated by fitting a polynomial through the acceptance differential cross section found from the least-squares procedure and integrating over each bin. In this procedure changes in the values of the $\theta_{\text{c.m.}}$ bin limits caused by the nonlinearities in the reconstruction matrix were also corrected. Off-line nonlinearity corrections for $\theta_{\text{c.m.}}$ and ϕ were only applied to the data sets I and II. For the other data sets the nonlinearity corrections were applied on-line for each event by the procedure which we have already described. The coefficients $\bar{f}_{nn}$, $\bar{f}_{ss}$, $\bar{f}_{sk}$, $\bar{f}_{ks}$, and $\bar{f}_{kk}$ of Eq. (12) were calculated by using the components of beam and target polarization as calculated by the tracking program and the values

of $\langle \sin\phi \rangle$, $\langle \cos\phi \rangle$, $\langle \cos^2\phi \rangle$, $\langle \sin^2\phi \rangle$, and $\langle \sin\phi \cos\phi \rangle$ for the appropriate ranges given in Table I.

A beam-polarization monitor with CH_2 target was used to measure the polarization of the accelerated beam. An absolute calibration of this monitor was performed by an independent measurement of the beam polarization at one energy. For this purpose, data were taken with two unpolarized-target positions $(+,0)$ and $(-,0)$ where the beam was vertically polarized. In this case, Eq. (11) reduces to

$$N_{+0}=\sigma_0(\theta)\bar{G}(\theta)[1+P(\theta)P_b]$$

and (21)

$$N_{-0}=\sigma_0(\theta)\bar{G}(\theta)[1-P(\theta)P_b]\ .$$

The ratio over the difference and sum of Eq. (21) gives $P_bP(\theta)$. The P parameter is well known from the phase shifts with an accuracy up to 1%. Therefore it was possible to extract P_b and its value was found to be $(85\pm2)\%$, which agreed very well with the measurements of the beam-polarization monitor.

D. Consistency tests and systematic errors

The data for each energy were subjected to a number of consistency tests and checks. For each solenoid setting, the quantity

$$P_t(+)/P_t(-)=(N_{P_b,+}-N_{P_b,0})/(N_{P_b,0}-N_{P_b,-}) \quad (22)$$

[where $P_t(+)$ and $P_t(-)$, are, respectively, the target polarization of the plus and minus runs] could be calculated from the data. This was not a very sensitive test because of the large errors on this calculated ratio. However, reasonable agreement was found between NMR values and this ratio. It was also possible to calculate the ratio of the two acceptances directly from the data for runs of different solenoid settings for checking the stability. The target polarization for each run was determined by averaging the measured NMR values over the duration of the run.

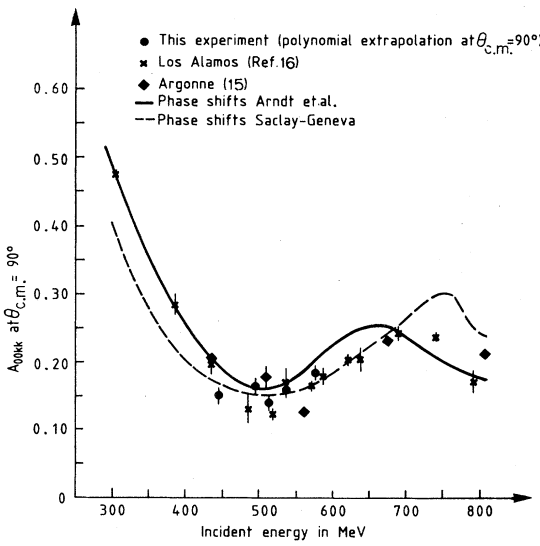

FIG. 6. A comparison of A_{00kk} values at $\theta_{c.m.}=90°$ with the measurements of Argonne (Ref. 15) and Los Alamos (Ref. 16).

There was a possible relative systematic error of $\pm$ (6% to 10%), due to the uncertainties in the NMR calibration as shown in Table II. As a check of the background subtraction, A_{pq} was also determined with several cuts on the S^2 distribution of the data. No significant changes were observed indicating that little or no background contamination remained in the data.

VII. RESULTS AND DISCUSSION

The results of A_{pq} vs $\theta_{c.m.}$ at 445 MeV are shown as an example in Fig. 4 for each set along with predictions for this parameter from the Saclay-Geneva phase-shift program[14] (dashed curve). The numerical values for A_{pq} at all energies are given in Table II with purely statistical errors. We also provide a relative systematic error for each set of data due to the fluctuation of target and/or beam polarizations.

To see the effects of these new measurements on the phase-shift predictions, these results were admitted into the Saclay-Geneva program and new values were generated. Significant modifications in A_{pq} were observed at all energies and are shown in Fig. 4 as a solid line. The introduction of these points into the program caused a reduction of about a factor of 2 in the phase-shift errors, indicating a substantial improvement in the reliability of the phase-shift predictions.

At 577 MeV, the sets I, II, III, and V cover the angular region of $\theta_{c.m.}=38°$ to 60°. For this domain we have extracted the values of A_{00kk}, A_{00ks}, and A_{00ss} by a linear fit as shown in Fig. 5(a). This fit gave $\chi^2=4.3$ per point indicating that one should take into account the systematic uncertainties due to the fluctuation of target and/or beam polarization. Therefore, we have added the systematic errors quadratically to the statistical errors and the errors on A_{00kk}, A_{00ks}, and A_{00ss} have increased from $(1-2)\%$ to $(3-4)\%$. This fit then gives $\chi^2=1.6$ per point. Data sets II, IV, and V cover the angular range between $\theta_{c.m.}=62°-90°$. For this domain we have extracted the values of the individual parameters by using an exact solution of the linear equations. At 514 MeV, we had the same sets as above with the linear fit giving $\chi^2=0.74$ per point. We had only data sets I, II, IV, and V at 536 and

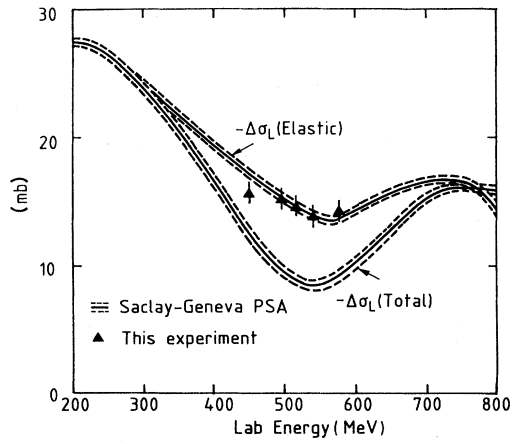

FIG. 7. Longitudinally polarized cross-section differences $(-\Delta\sigma_L)$ and their elastic content.

TABLE III. Values of A_{00kk}, A_{00ks}, and A_{00ss} at five energies as extracted from the data of Table II.

$\theta_{c.m.}$ (deg)	A_{ss}	A_{sk}	A_{kk}
		577 MeV	
38	−0.370±0.020	−0.185±0.023	0.413±0.036
42	−0.380±0.020	−0.166±0.021	0.390±0.035
46	−0.410±0.022	−0.117±0.019	0.348±0.033
50	−0.419±0.022	−0.106±0.019	0.341±0.033
54	−0.445±0.024	−0.107±0.019	0.324±0.032
56	−0.498±0.050	−0.077±0.021	0.318±0.032
58	−0.477±0.055	−0.068±0.022	0.319±0.032
62	−0.573±0.047	−0.028±0.014	0.300±0.035
66	−0.562±0.046	−0.019±0.014	0.257±0.032
70	−0.601±0.047	−0.010±0.014	0.236±0.031
74	−0.547±0.045	−0.016±0.014	0.209±0.028
78	−0.588±0.047	−0.001±0.015	0.327±0.031
82	−0.619±0.048	+0.019±0.016	0.163±0.027
86	−0.607±0.049	−0.009±0.016	0.216±0.030
90	−0.627±0.047	+0.048±0.017	0.183±0.030
		536 MeV	
38	−0.407±0.071	−0.194±0.023	0.430±0.034
42	−0.375±0.067	−0.187±0.022	0.421±0.032
46	−0.434±0.068	−0.182±0.021	0.430±0.032
50	−0.436±0.067	−0.157±0.020	0.378±0.030
54	−0.453±0.067	−0.135±0.019	0.384±0.030
56	−0.516±0.068	−0.101±0.018	0.358±0.030
58	−0.571±0.068	−0.071±0.017	0.333±0.029
62	−0.613±0.061	−0.079±0.012	0.309±0.029
66	−0.542±0.057	−0.056±0.016	0.255±0.031
70	−0.561±0.060	−0.066±0.017	0.272±0.030
74	−0.532±0.060	−0.048±0.017	0.213±0.032
78	−0.626±0.060	−0.021±0.017	0.199±0.033
82	−0.608±0.060	−0.037±0.018	0.126±0.033
86	−0.609±0.061	−0.032±0.018	0.174±0.035
90	−0.667±0.063	+0.002±0.018	0.193±0.038
		514 MeV	
38	−0.342±0.029	−0.260±0.026	0.498±0.034
42	−0.369±0.030	−0.222±0.020	0.463±0.031
46	−0.394±0.031	−0.202±0.020	0.489±0.031
50	−0.437±0.033	−0.169±0.018	0.443±0.030
54	−0.450±0.034	−0.139±0.014	0.352±0.027
56	−0.494±0.034	−0.118±0.014	0.348±0.027
58	−0.509±0.038	−0.122±0.012	0.366±0.027
62	−0.569±0.054	−0.115±0.012	0.276±0.025
66	−0.571±0.050	−0.062±0.014	0.273±0.027
70	−0.563±0.052	−0.078±0.014	0.231±0.026
74	−0.633±0.053	−0.051±0.014	0.245±0.028
78	−0.604±0.052	−0.042±0.015	0.158±0.028
82	−0.649±0.054	−0.040±0.015	0.123±0.028
86	−0.629±0.051	−0.007±0.016	0.159±0.030
90	−0.589±0.052	−0.015±0.017	0.151±0.031
		494 MeV	
38	−0.380±0.068	−0.249±0.028	0.574±0.037
42	−0.414±0.063	−0.270±0.025	0.585±0.035
46	−0.472±0.059	−0.211±0.022	0.545±0.033
50	−0.561±0.057	−0.164±0.021	0.518±0.033
54	−0.543±0.055	−0.154±0.020	0.470±0.031
56	−0.559±0.055	−0.138±0.020	0.465±0.032

TABLE III. *(Continued.)*

$\theta_{c.m.}$ (deg)	A_{ss}	A_{sk}	A_{kk}
58	−0.563±0.054	−0.129±0.020	0.464±0.031
62	−0.585±0.047	−0.104±0.015	0.404±0.029
66	−0.642±0.050	−0.090±0.019	0.368±0.031
70	−0.683±0.051	−0.058±0.020	0.319±0.032
74	−0.664±0.051	−0.053±0.020	0.272±0.031
78	−0.711±0.050	−0.003±0.021	0.195±0.031
82	−0.687±0.050	+0.003±0.021	0.187±0.032
86	−0.693±0.050	−0.020±0.021	0.191±0.032
90	−0.712±0.050	+0.024±0.021	0.151±0.034
	445 MeV		
38	−0.409±0.027	−0.267±0.021	0.520±0.030
42	−0.440±0.026	−0.248±0.015	0.506±0.026
46	−0.480±0.027	−0.202±0.015	0.572±0.026
50	−0.508±0.027	−0.179±0.014	0.455±0.023
54	−0.546±0.028	−0.155±0.013	0.450±0.023
56	−0.590±0.050	−0.117±0.017	0.423±0.024
58	−0.594±0.050	−0.098±0.017	0.405±0.024
62	−0.494±0.050	−0.129±0.018	0.379±0.026
66	−0.568±0.049	−0.111±0.017	0.375±0.038
70	−0.598±0.050	−0.070±0.018	0.281±0.025
74	−0.533±0.059	−0.082±0.018	0.262±0.029
78	−0.743±0.063	−0.014±0.019	0.207±0.031
82	−0.635±0.061	−0.034±0.019	0.195±0.031
86	−0.681±0.062	−0.020±0.019	0.132±0.031
90	−0.673±0.064	+0.020±0.019	0.116±0.034

494 MeV with set V having been measured twice, once with an accelerated beam and once with a scattered beam at the latter energy. At 445 MeV, we had eight sets, namely, sets I, II, IV–IX. Sets VI and VII had more or less the same combination as sets II and V, respectively, but some normalization problems between the two were observed. The reasons for the discrepancy, after a careful and detailed analysis was found to be some instabilities in a few runs of the former sets. Corrections were made, after which a good agreement was found. An average χ^2 of 0.4 over the eight sets of data was obtained.

The results for A_{00kk}, A_{00ks}, and A_{00ss} as a function of $\cos^2\theta_{c.m.}$ for the various energies are shown in Fig. 5 and Table III, along with A_{00nn} results from our earlier experiment (further measurements on A_{00nn} made recently at 577 MeV were added to these data). The dashed curves are the predictions of the Saclay-Geneva phase shifts and the solid line shows the changes in the predictions after these results were admitted into this phase-shift program. Our results verify the symmetry constraints at $\theta_{c.m.}=90°$, namely, $A_{00nn}-A_{00ss}-A_{00kk}=1$ and $A_{00ks}=0$ at all energies.

A comparison of our A_{00kk} values at $\theta_{c.m.}=90°$ with the measurements of Argonne[15] and Los Alamos[16] are shown in Fig. 6. For this, we have fitted our A_{00kk} values with a polynomial of the type $(a+b\cos^2\theta_{c.m.})$ to smooth the data and the results are shown in Table IV. The agreement of the A_{00kk} values with the data of Argonne and Los Alamos at all energies is reasonably good.

Recently, we have measured the polarization parameter P, the two-spin-polarization transfer parameters D_{n0n0},K_{n00n} and $D_{s'0s0}$, $D_{s'0k0}$, and the three-spin parameters $M_{s'0sn}$,$M_{s'0kn}$ for p-p elastic scattering between 34° and 118° center of mass at 579 and 445 MeV (Refs. 17 and 18, respectively), thus totaling 15 observables (between 38° and 90°) and 11 observables (between 38° and 62°) with the

TABLE IV. Values of A_{00kk}, A_{00ss}, and A_{00nn} at $\theta_{c.m.}=90°$, extrapolated from a fit $(a+b\cos^2\theta_{c.m.})$ over the values of the neighboring $\theta_{c.m.}$ angles. Total error is given by total error=statistical error + quadratic addition of systematics errors and shown in parentheses.

Energy (MeV)	$A_{00ss}\pm\Delta A_{00ss}$ at $\theta_{c.m.}=90°$	$A_{00kk}\pm\Delta A_{00kk}$ at $\theta_{c.m.}=90°$	$A_{00nn}\pm\Delta A_{00nn}$ at $\theta_{c.m.}=90°$	Symmetry relations at 90° c.m. $A_{nn}-A_{ss}-A_{kk}=1$
445	−0.661±0.022(0.038)	0.150±0.015(0.017)	0.499±0.019	1.01 ±0.032(0.054)
494	−0.713±0.021(0.030)	0.167±0.016(0.021)		
514	−0.636±0.020(0.045)	0.140±0.015(0.018)	0.495±0.014	0.991±0.029(0.051)
536	−0.625±0.025(0.040)	0.159±0.017(0.019)	0.534±0.012	1.00 ±0.033(0.050)
577	−0.611±0.018(0.036)	0.187±0.015(0.026)	0.555±0.021	0.980±0.031(0.054)

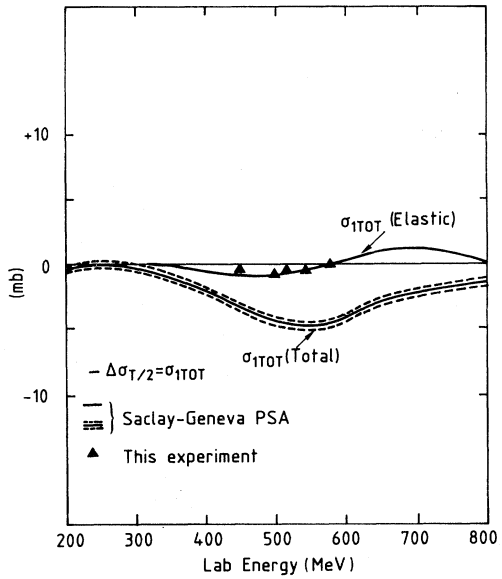

FIG. 8. Transversely polarized cross-section differences ($\sigma_{1\,\mathrm{tot}}=-\Delta\sigma_T/2$) and their elastic content.

spin-correlation parameters presented in this article. These observables, together with the differential cross section, have allowed a model-independent determination of the scattering matrix.[19,20] There was a very good compatibility between the spin-correlation parameters and the other parameters used in these analyses.[20,21]

The observed structure in the p-p total-cross-section differences ($\Delta\sigma_L$) was the essential evidence in favor of dibaryon resonances[1,2,22] and the preliminary data from the Geneva-Saclay collaboration has confirmed the significant structure observed by the Argonne group in the overlapping energy region.[4] Still there is a great controversy over the interpretation of these results. It has been suggested that this structure could be due to strongly inelastic dibaryon resonances, but the case is yet unproven. An equally likely explanation is that the $\Delta(1230)$ doorway state in πd and strong inelastic thresholds in the pp-$NN\pi$ are responsible for the oscillations in ($\Delta\sigma_L$) and ($\Delta\sigma_T$).[23]

We have estimated the elastic contribution for the transversely and longitudinally polarized cross-section differences by using the relation below:

$$\sigma_{1\mathrm{tot}}=-\tfrac{1}{2}\pi\int_0^{\pi}(d\sigma/d\Omega)(A_{00nn}+A_{00ss})\sin\theta\,d\theta\,, \tag{23}$$

$$\Delta\sigma_L=-2\pi\int_0^{\pi}(d\sigma/d\Omega)A_{00kk}\sin\theta\,d\theta\,. \tag{24}$$

TABLE V. Estimation of the elastic content of the longitudinally and transversely polarized cross-section differences $\Delta\sigma_L$ and $\Delta\sigma_T$. Errors are statistical only.

Energy (MeV)	Elastic $\Delta\sigma_L$ (mb)	Elastic $\Delta\sigma_T$ (mb)
577	−14.7±0.7	0.11±0.14
536	−14.3±0.4	−1.20±0.10
514	−14.0±0.3	−1.43±0.08
494	−15.6±0.3	−1.53±0.08
445	−15.9±0.4	−0.80±0.20

The spin-correlation parameters presented in this paper are used to calculate the elastic part of $\Delta\sigma_L$ and $\Delta\sigma_T$. Our measurements of the elastic channel which cover the angular range between 36° and 90° allow a good approximation of these integrals, since the remaining solid angle between 0° and 36° is only $\simeq$19% of the total solid angle. Moreover, for the range between 0° and 36°, we have used the predictions of phase-shift analysis (PSA's) which included D, R, and A parameters at small angles.[24] We present the results of these calculations along with the predictions of the Saclay-Geneva PSA for $\Delta\sigma_L$,$\sigma_{1\mathrm{tot}}$ (total, elastic) in Figs. 7 and 8 and Table V.

ACKNOWLEDGMENTS

We would like to thank Dr. D. Besset and the many members of the Swiss Institute for Nuclear Research without whom this experiment would have been impossible. We would like to acknowledge the support and continued interest of Professor J. P. Blaser, Director of SIN. Special thanks go to Professor R. Mermod for his constant encouragement during this research. We are indebted to the technical staff of the University of Geneva for their invaluable help and outstanding technical assistance. This work was supported by the Swiss National Science Foundation and the Convention Intercantonale d'Enseignement du Troisième Cycle de la Physique en Suisse Romande.

*Present address: High Energy Physics Lab., Harvard University, Cambridge, MA 02138.

†Present address: Physics Department, University of California, Irvine, CA 92717.

[1]I. P. Auer, E. Colton, H. Halpern, D. Hill, H. Spinka, G. Theodosiou, D. Underwood, Y. Watanabe, and A. Yokosawa, Phys. Lett. 67B, 113 (1977).

[2]I. P. Auer, A. Beretvas, E. Colton, D. Hill, K. Nield, H. Spinka, D. Underwood, Y. Watanabe, and A. Yokosawa, Phys. Lett. 70B, 475 (1977).

[3]I. P. Auer, E. Colton, H. Halpern, D. Hill, H. Spinka, and G. Theodosiou, D. Underwood, Y. Watanabe, and A. Yokosawa, Phys. Rev. Lett. 41, 354 (1978).

[4]E. Aprile, J. Bystricky, J. Deregel, C. Eisenegger, J. M. Fontaine, E. Heer, R. Hess, F. Lehar, W. Leo, S. Mango, Y. Onel, F. Perrot, D. Rapin, J. Vrzal, and J. Yonnet, in *High Energy Physics with Polarized Beams and Polarized Targets,* proceedings of the International Symposium, Lausanne, Switzerland, 1980, edited by C. Joseph and J. Soffer (Birkhauser, Basel, Switzerland and Boston, 1981).

[5]M. L. Marshak, in *High Energy Physics with Polarized Beams and Polarized Targets,* proceedings of the International Symposium, Lausanne, Switzerland, 1980, edited by C. Joseph and J. Soffer (Birkhauser, Basel, Switzerland and Boston, 1981).

[6]R. Vinh-Mau, in *Nucleon-Nucleon Interactions—1977,* Proceedings of the Second International Conference on Nucleon-Nucleon Interactions, Vancouver, edited by Harold Fearing, David Measday, and Ada Strathdee (AIP, New

York, 1978).

[7]D. Besset, Q. H. Do, B. Favier, R. Hausammann, E. Heer, R. Hess, C. Lechanoine-LeLuc, W. Leo, D. Rapin, D. W. Werren, Ch. Weddigen, J. M. Cameron, S. Jaccard, and S. Mango, Nucl. Phys. A345, 435 (1980).

[8]D. Besset, Q. H. Do, B. Favier, L. G. Greeniaus, E. Heer, R. Hess, C. Lechanoine-LeLuc, D. Rapin, D. W. Werren, M. Daum, S. Mango, E. Steiner, G. Vecsey, and C. Weddigen, Nucl. Instrum. Methods 184, 365 (1981).

[9]S. Mango, O. Runolfsen, and M. Borghini, Nucl. Instrum. Methods 72, 45 (1965).

[10]D. Besset, Ph.D. thesis No. 1882, Université de Geneve, 1978 (unpublished).

[11]J. Bystricky, F. Lehar, and P. Winternitz, J. Phys. (Paris) 39, 1 (1978).

[12]E. Aprile, R. Hausammann, E. Heer, R. Hess, C. Lechanoine-LeLuc, W. Leo, Y. Onel, and D. Rapin, Topical Conference on the Application of Microprocessors to High Energy Physics Experiments, CERN Yellow Report No. 81-07 (unpublished), p. 124.

[13]R. Hausammann, E. Heer, R. Hess, C. Lechanoine-LeLuc, W. Leo, Y. Onel, D. Rapin, and S. Mango, in *Proceedings of the Eighth International Conference on High Energy and Nuclear Structure,* edited by D. F. Measday and A. W. Thomas (North-Holland, Amsterdam, 1980).

[14]J. Bystricky, F. Lehar, and C. Lechanoine-LeLuc, Saclay Report No. 79.01, 1979 (unpublished).

[15]J. Bystricky and F. Lehar, No. 11-1 of *Physics Data* (Fachinformationzentrum, Karlsruhe, 1978).

[16]S. J. Stuart, Los Alamos Report No. LA-9504-T, 1982 (unpublished).

[17]E. Aprile, C. Eisenegger, R. Hausammann, E. Heer, R. Hess, C. Lechanoine-LeLuc, W. Leo, Y. Onel, D. Rapin, and S. Mango, in *High Energy Physics with Polarized Beam and Polarized Targets* (Ref. 5).

[18]E. Aprile-Giboni, G. Cantale, R. Hausammann, E. Heer, R. Hess, C. Lechanoine-LeLuc, W. R. Leo, S. Morenzoni, Y. Onel, D. Rapin, and S. Mango, in *High Energy Spin Physics—1982,* proceedings of the Fifth International Symposium, Brookhaven National Laboratory, edited by G. M. Bunce (AIP, New York, 1983).

[19]E. Aprile, R. Hausammann, E. Heer, R. Hess, C. Lechanoine-LeLuc, W. Leo, S. Morenzoni, Y. Onel, D. Rapin, and S. Mango, in *High Energy Spin Physics—1982* (Ref. 18).

[20]E. Aprile, C. Eisenegger, R. Hausammann, E. Heer, R. Hess, C. Lechanoine-LeLuc, W. Leo, S. Morenzoni, Y. Onel, D. Rapin, and S. Mango, Phys. Rev. Lett. 46, 1047 (1981).

[21]R. Hess, in *High Energy Physics with Polarized Beams and Polarized Targets* (Ref. 5).

[22]N. Hoshizaki, Prog. Theor. Phys. 60, 1790 (1978).

[23]D. V. Bugg, in *High Energy Physics with Polarized Beams and Polarized Targets* (Ref. 5).

[24]D. Besset, Q. H. Do, B. Favier, L. G. Greeniaus, R. Hess, C. Lechanoine, D. Rapin, D. W. Werren, and C. H. Weddigen, Phys. Rev. D 21, 580 (1980).

[25]W. Grein and P. Kroll, Nucl. Phys. B137, 173 (1978).